# **PCCP**



**PAPER** 

View Article Online
View Journal | View Issue



Cite this: *Phys. Chem. Chem. Phys.*, 2023, **25**, 21065

# Lithium transference in electrolytes with star-shaped multivalent anions measured by electrophoretic NMR†

Saheli Chakraborty, (\*\*D\pm\*) \pm^abc\* David M. Halat, (\*\*D\pm\*) \pm\* Julia Im, (\*\*D\pm\*)

Darby T. Hickson, (\*\*D\pm\*) abc\* Jeffrey A. Reimer (\*\*D\pm\*) and Nitash P. Balsara (\*\*D\pm\*) \*\*abc\*

One approach for improving lithium transference in electrolytes is through the use of bulky multivalent anions. We have studied a multivalent salt containing a bulky star-shaped anion with a polyhedral oligomeric silsesquioxane (POSS) center and lithium counterions dissolved in a solvent. The charge on each anion,  $z_{-}$ , is equal to -20. The self-diffusion coefficients of all species were measured by pulsed field gradient NMR (PFG-NMR). As expected, anion diffusion was significantly slower than cation diffusion. An approximate transference number, also referred to as the current fraction (measured by Bruce, Vincent and Watanabe method), was higher than those expected from PFG-NMR. However, the rigorously defined cation transference number with respect to the solvent velocity measured by electrophoretic NMR was negative at all salt concentrations. In contrast, the approximate transference numbers based on PFG-NMR and current fractions are always positive, as expected. The discrepancy between these three independent approaches for characterizing lithium transference suggests the presence of complex cation—anion interactions in solution. It is evident that the slow self-diffusion of bulky multivalent anions does not necessarily lead to an improvement of lithium transference.

Received 28th February 2023, Accepted 27th June 2023

DOI: 10.1039/d3cp00923h

rsc.li/pccp

#### Introduction

There is significant interest in multivalent electrolytes due to their relevance in rechargeable batteries. <sup>1-6</sup> Electrolytes used in lithium-ion batteries comprise univalent ions dissolved in a mixture of organic solvents. Lithium transference in these electrolytes is low, implying that a large fraction of current is carried by the anions. <sup>7,8</sup> It has been postulated that bulky multivalent anions may lead to an improvement of lithium transference. <sup>9-11</sup> In a recent study, Nguyen *et al.* studied ion transport in solutions containing bulky multivalent star-shaped anions where one also expects ion transport to be dominated by that of the cation. <sup>1</sup>

Irrespective of the valency of the ions, the performance of binary electrolytes, comprising two ions and a solvent, in batteries depends on three transport parameters: ionic conductivity,

$$\rho_+ = \frac{i_{\rm ss}}{i_0}.\tag{1}$$

Eqn (1) is valid when the current through the cell is dominated by bulk impedance (not interfacial impedance). While the currents depend on the magnitude of  $\Delta\phi$ ,  $\rho_+$  is a material property that is independent of  $\Delta\phi$  when the applied potentials are sufficiently small. Another approach for determining the transference number employs pulsed field gradient NMR (PFG-NMR) which can be used to measure the self-diffusion coefficients of the cations and anions,  $D_+$  and  $D_-$ . <sup>18</sup> The PFG-NMR-based cation

 $<sup>\</sup>kappa$ , salt diffusion coefficient, D, and cation transference number,  $t_+^0$ . The purpose of this paper is to study lithium transference in a solution comprising star-shaped multivalent anions presenting a valency of -20, univalent Li<sup>+</sup> counterions, and a low molar mass solvent – a mixture of ethylene carbonate (EC) and dimethyl carbonate (DMC). The transference number,  $t_+^0$ , is defined as the fraction of current carried by the cation relative to the solvent velocity. The most popular approach to study lithium transference is one wherein the electrolyte is sandwiched between two lithium metal electrodes and the current i under a steady applied potential  $\Delta \phi$  is monitored as a function of time. Following the work of Bruce, Vincent, and Watanabe et al., al. we define the current ratio al. as the ratio of the steady state current al. to that of the initial current al.

<sup>&</sup>lt;sup>a</sup> Materials Sciences Division, Lawrence Berkeley National Laboratory, Berkeley, California 94720, USA. E-mail: nbalsara@berkeley.edu

b Department of Chemical and Biomolecular Engineering, University of California, Berkeley, Berkeley, California 94720, USA

<sup>&</sup>lt;sup>c</sup> Joint Center for Energy Storage Research (JCESR), Lawrence Berkeley National Laboratory, Berkeley, California 94720, USA

 $<sup>\</sup>dagger$  Electronic supplementary information (ESI) available. See DOI: https://doi.org/10.1039/d3cp00923h

<sup>‡</sup> Both the authors contributed equally.

**Paper** 

transference number can be defined as

$$t_{+,PFG} = \frac{z_{+}D_{+}}{z_{+}D_{+} - z_{-}D_{-}}.$$
 (2)

Here,  $z_i$  represents the charge on species j (valency).<sup>19</sup>

In the limit of infinite dilution,  $t_+^0$ ,  $\rho_+$ , and  $t_{+,PFG}$  must be equal to each other. 20,21 At finite concentrations, however, the relationships between these parameters are nontrivial; they depend on other transport and thermodynamic parameters that reflect correlations between different species. 12,22

An alternative approach for measuring  $t_{+}^{0}$  is electrophoretic NMR (eNMR). 23-32 In this approach, pioneered by Zawodinski and coworkers,  $^{27,28}$  a steady electric potential  $\Delta \phi$  is applied across the electrolyte and the displacement of the NMR-active species in a fixed time window is measured by quantifying spectral phase shifts. This enables determining species velocities that are directly related to  $t_{+}^{0}$ . In the case of univalent ions,24,25 it was shown that

$$t_{+}^{0} = \frac{v_{+} - v_{0}}{v_{+} - v_{-}}.$$
 (3)

Here,  $v_+$ ,  $v_-$  and  $v_0$  are the average velocities of the cation, anion and solvent, respectively. While the species velocities are proportional to  $\Delta \phi$ ,  $t_{+}^{0}$  is a dimensionless material property that is independent of  $\Delta \phi$  when the applied potentials are sufficiently small.

The salt we have chosen for our study is lithiated polyhedral oligomeric silsesquioxane (POSS) nanoparticles (Fig. 1). These nanoparticles can be thought of as eight-armed stars with two or three anions in each arm, yielding  $z_{-} = -20$ . A similar salt with  $z_{-}$  ranging from 6.6 to 10 was studied by Bouchet and coworkers where they report high PFG-NMR-based cation transference numbers. While the star-shaped anions are similar to charged dendrimers that have been studied in previous literature, 33-38 we are not aware of any measurements of transference in solutions of such systems. In the present work, our main objective is to study the relationship between  $t_+^0$ ,  $\rho_+$ , and  $t_{+,PFG}$  in our multivalent POSS system.

## **Experimental section**

#### Preparation of the electrolyte

The POSS nanoparticles containing lithium salt of polystyrene-4-sulfonyl(trifluoromethane sulfonyl) imide (POSS-PSLiTFSI) were synthesized following the previous literature report.<sup>39</sup> The salty nanoparticles were dried at 100 °C under active vacuum for 72 hours. The salt was stored under argon in a glovebox where water and oxygen levels were kept below 0.5 ppm before further use.

The electrolytes were prepared inside the glovebox by adding the required amount of POSS-PSLiTFSI to the dry ethylene carbonate (EC) and dimethyl carbonate (DMC) mixture (1:1 by weight) and the solution was stirred at 60 °C overnight in an airtight container.

The concentrations of the electrolytes were determined by NMR spectroscopy. The <sup>7</sup>Li NMR spectra of solutions of LiTFSI salt in N-methylpyrrolidone with concentrations ranging from 0.05 to 1 mol  $L^{-1}$  were recorded and the peak intensities were used to generate a calibration curve. A recycle delay period of 5 s was applied between each NMR scan to ensure the complete relaxation of the species. A total of 8 scans were performed in each NMR experiment. The calibration curve is shown in Fig. 2. Mixtures of POSS-PSLiTFSI/EC/DMC with known mass fractions of POSS-PSLiTFSI were prepared and the <sup>7</sup>Li peak intensities from these solutions were measured. The measured intensities were compared with the calibration curve as shown in Fig. 2 and this enabled determining the molar concentrations of lithium ions,  $c_+$ . The  $c_+$  values thus obtained are 0.071, 0.21, 0.40, 0.53 and  $0.73 \text{ mol L}^{-1}$ . These NMR experiments also enable the calculation of the average number of lithium ions per POSS particle in each electrolyte. Data obtained from all five solutions were used to determine the average valency of the anions. This analysis gave  $z_{-}$  =  $-20 \pm 2$ . This implies that the average number of monomers per chain is 2.5 assuming that the chains emanate from all eight corners of the POSS particles.

#### **Electrochemical characterization**

Conductivity measurements. The conductivity of the electrolytes were measured using a Mettler Toledo InLab-751 conductivity probe with platinum blocking electrodes. The temperature of

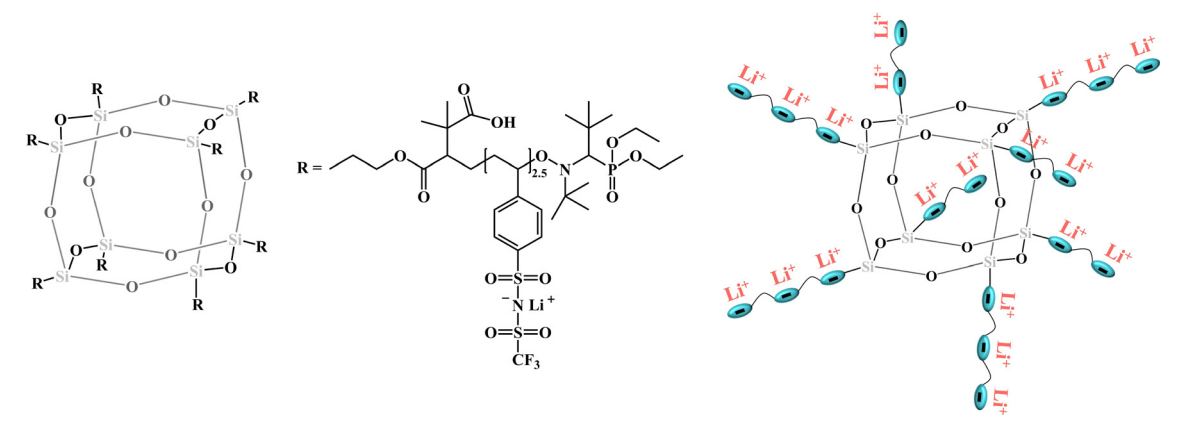


Fig. 1 Chemical formula of the polyanionic electrolyte based on POSS. The average number of negative charges on the POSS nanoparticle is 20.

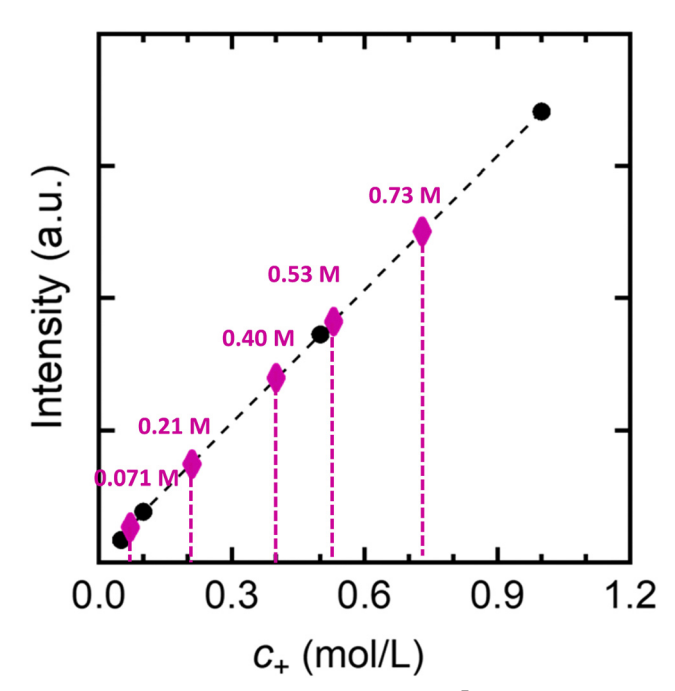


Fig. 2 Determination of salt concentration by <sup>7</sup>Li NMR spectroscopy. The y-axis represents the intensity of the NMR spectra and the x-axis represents the concentration of lithium salt. The data points in black circles and the connected black dotted lines represent the calibration curve with different LiTFSI salt concentrations. Magenta diamonds represent the POSS-PSLiTFSI data and the vertical lines to the x-axis represent the determined concentrations. The numbers in the figure represent  $c_{+}$  of the electrolytes used in this study.

the electrolytes was measured using the probe and was maintained at 30  $\pm$  1  $^{\circ}$ C during measurements. Each measurement was carried out three times to ensure reproducibility. The conductivity probe was calibrated prior to the experiment using a potassium chloride standard with a conductivity of 1413 μS cm<sup>-1</sup> to determine the cell constant.

Current fraction measurement. The current fraction was determined using Li/POSS-PSLiTFSI(EC/DMC)/Li symmetric cells assembled in coin cell conformation. Five layers of Celgard 2500 separators were soaked in the electrolyte and stacked between lithium chips of 14 mm in diameter and 600 µm in thickness (MTI Corp.). The cell stack was backed with a stainless-steel shim of diameter 15.5 mm and a wave spring before crimping. At least three to four cells were made at each salt concentration to check reproducibility. The cells were cycled at 30 °C inside an environmental chamber connected to a thermocouple.

The cells were preconditioned by polarizing at 0.02 mA cm<sup>-2</sup> for four hours in both positive and negative directions followed by one hour of open circuit potential relaxation steps between each of the polarization steps. Five preconditioning cycles were carried out to ensure the formation of a stable solid electrolyte interphase (SEI) between the lithium metal and the electrolyte. After this, the cells were polarized at  $\Delta \phi = 10$  mV, -10 mV, 20 mV and -20 mV to ensure that the measurements were independent of the applied potential. The steady state current,  $i_{ss}$ , was measured for 1 h and the impedance was monitored before  $(R_{b,0}, R_{i,0})$ 

and after the polarization ( $R_{b,ss}$  and  $R_{i,ss}$ ).  $R_b$  and  $R_i$  represent the bulk and interfacial resistances, respectively. The initial current density is determined based on Ohm's law assuming the absence of any concentration gradient at the initial instant of polarization as

$$i_{\Omega} = \frac{\Delta \phi}{R_{\rm i,0} + R_{\rm b,0}}.\tag{4}$$

The current fraction was determined using the following equation15-17

$$\rho_{+} = \frac{i_{ss}}{i_{\Omega}} \left( \frac{\Delta \phi - i_{\Omega} R_{i,0}}{\Delta \phi - i_{ss} R_{i,ss}} \right). \tag{5}$$

Eqn (5) is an extension of eqn (1) for the case when interfacial impedance cannot be neglected.

Pulsed-field-gradient NMR. All <sup>7</sup>Li, <sup>19</sup>F, and <sup>1</sup>H NMR experiments were performed at a field strength of 9.4 T using a 400 MHz Bruker NEO spectrometer and a Bruker 5 mm watercooled double resonance broadband diffusion (diffBB) probe, which was equipped with z-axis gradient capabilities permitting a maximum gradient strength of 17 T m<sup>-1</sup> and variabletemperature control. The observed <sup>7</sup>Li and <sup>19</sup>F resonances unambiguously corresponded to Li<sup>+</sup> cations and polyanions, respectively; the <sup>1</sup>H resonances corresponding to the carbonate solvents were chosen for analysis. For PFG experiments, a standard stimulated-echo sequence (diffSte) using sine-bell magnetic field gradient pulses was employed, wherein only the gradient strength was varied for each measurement; spoiler gradient pulses of 2 ms and a longitudinal eddy current delay (LED) period of 20 ms were used for all experiments. Additionally, dummy gradient pulses were performed prior to the first spectral acquisition. Typical <sup>19</sup>F, <sup>7</sup>Li and <sup>1</sup>H PFG parameters, *i.e.*, gradient pulse length ( $\delta$ ), diffusion time ( $\Delta$ ), and maximum gradient strength (g), were equal to or ranged as follows:  $\delta$  = 1 ms,  $\Delta = 20$  ms, g = 1.4-5.3 T m<sup>-1</sup> (<sup>1</sup>H);  $\delta = 1.5$  ms,  $\Delta = 50$  ms,  $g = 2.0-12.8 \text{ T m}^{-1} (^{19}\text{F}); \text{ and } \delta = 1 \text{ ms}, \Delta = 50 \text{ ms}, g = 4.1-$ 9.8 T m<sup>-1</sup> (<sup>7</sup>Li). All measurements were performed at a calibrated sample temperature of 30 °C. Temperature and pulsed field gradient strength calibrations were performed with a standard consisting of 80% ethylene glycol in DMSO-d6 (Cambridge Isotope Labs), using the known <sup>1</sup>H self-diffusion coefficient of ethylene glycol at the calibrated temperature.<sup>40</sup> Data were processed and analyzed in Bruker TopSpin 3.6 and/or 4.1, and Bruker Dynamics Center.

Electrophoretic NMR. The electrophoretic NMR (eNMR) instrumentation employed in this work was based on the setup described by Fang et al.,41 and was supplied by P & L Scientific Instrument Service (https://www.plscientific.se; Lidingö, Sweden); details of our eNMR measurements have been previously reported in detail.<sup>25</sup> All electrolyte samples were loaded into the eNMR cell within the argon-filled glovebox used for electrolyte preparation; the cells were previously dried at 60 °C overnight. We used a convection-compensated double stimulated-echo (DSTE) PFG-NMR sequence, 42 with electric field pulses of opposite polarity applied during the two halves of the sequence. 43-45 Typical applied voltages ranged from 10 to 160 V. Although a range of electric fields were applied, in this work all eNMR species velocities are reported relative to an applied electric field of  $-1~V~mm^{-1}.$  For all experiments, the drift time  $\Delta$  during which the electric field was applied was fixed at 100 ms. Typical recycle delays were 60–120 s, to allow for equilibration following the electric field pulses. The calibrated sample temperature was 30  $^{\circ}\mathrm{C}$  for all measurements. Calibration of the electric field was previously performed with a 10 mM solution of tetramethylammonium bromide (TMABr) in  $D_2\mathrm{O}$  (supplied by P & L Scientific) at 25  $^{\circ}\mathrm{C}.$  Analysis of eNMR phase shifts was performed as previously described  $^{25}$  using an automated procedure comparing the "phase spectra" of the eNMR data.

#### Theory

In this section, we derive expressions that are necessary to interpret the experimental data from multivalent systems. Our derivations are built on the approach described in ref. 24. We assume that we have a one-dimensional system with a potential  $\Delta\phi$  applied across an electrolyte of length L (Fig. 3). We are interested in predicting the initial species velocities before the onset of concentration polarization. Under these conditions, the gradient of the electric field inside the electrolyte,  $\nabla\phi$ , is given by  $-\Delta\phi/L$ .

We use concentrated solution theory to derive the necessary equations.<sup>12</sup> In this theory, the Stefan-Maxwell approach is used to describe transport which is driven by the gradients of the electrochemical potentials,  $\mu_i$ . Eqn (10)–(12) from ref. 24 are

$$c_{+}\nabla\mu_{+} = \frac{RTc_{+}c_{0}}{c_{T}\mathcal{D}_{0+}}(v_{0} - v_{+}) + \frac{RTc_{+}c_{-}}{c_{T}\mathcal{D}_{+-}}(v_{-} - v_{+})$$
 (6)

$$c_{-}\nabla\mu_{-} = \frac{RTc_{-}c_{0}}{c_{T}\mathcal{D}_{0-}}(v_{0} - v_{-}) + \frac{RTc_{+}c_{-}}{c_{T}\mathcal{D}_{+-}}(v_{+} - v_{-})$$
 (7)

$$c_0 \nabla \mu_0 = \frac{RTc_- c_0}{c_T \mathcal{D}_{0-}} (\nu_- - \nu_0) + \frac{RTc_+ c_0}{c_T \mathcal{D}_{0+}} (\nu_+ - \nu_0)$$
 (8)

where  $\mathcal{D}_{jk}$  are Stefan–Maxwell diffusion coefficients,  $c_j$  is the species concentration, and  $c_T$  is the total solution concentration.

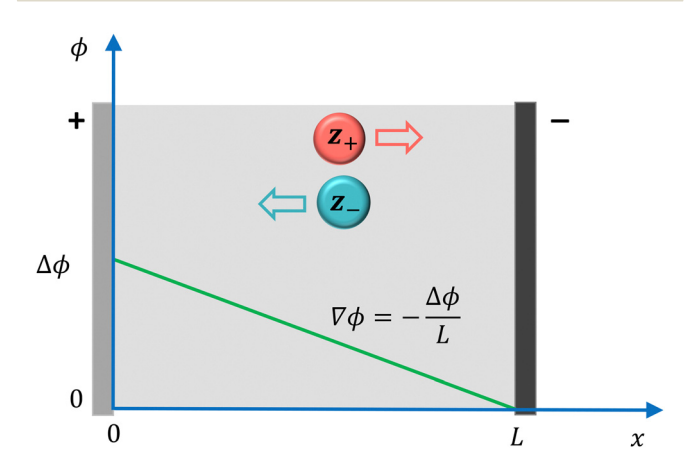


Fig. 3 Schematic of the eNMR cell where a positive potential  $\Delta\phi$  is applied at x=0. The potential of the negative electrode is set to zero. The direction of migration of the dissociated ions is shown by the arrows (red and blue). The potential gradient driving the ion motion is given. The solution concentration is uniform, independent of x.

The velocities given in eqn (6)–(8) reflect averages over all of the different environments (dissociated ions, ion pairs, solvent separated ion pairs, charged triplets, *etc.*). Molecular-scale simulations are usually used to identify these environments, and the correspondence between the continuum and molecular approaches has been established in several previous publications. <sup>25,46–49</sup>

Using quasi-electrostatic potentials in an electrolyte of a uniform composition, <sup>12</sup> we have

$$\nabla \mu_{+} = z_{+} F \nabla \phi \tag{9}$$

$$\nabla \mu_{-} = z_{-}F\nabla \phi \tag{10}$$

$$\nabla \mu_0 = 0 \tag{11}$$

Combining eqn (8) and (11), and noting that  $c_+ = c\nu_+$  and  $c_- = c\nu_-$ , where  $\nu_j$  is the moles of ions produced by the dissociation of one mole of the electrolyte, we get

$$\frac{\mathcal{D}_{0+}}{\mathcal{D}_{0-}} = -\frac{\nu_+(\nu_+ - \nu_0)}{\nu_-(\nu_- - \nu_0)} \tag{12}$$

The transference number is defined in terms of the Stefan-Maxwell diffusion coefficients as

$$t_{+}^{0} = \frac{z_{+}\mathcal{D}_{0+}}{z_{+}\mathcal{D}_{0+} - z_{-}\mathcal{D}_{0-}} \tag{13}$$

where  $z_j$  is the charge of species j. Substituting eqn (12) in eqn (13), and noting that  $z_+\nu_+ = -z_-\nu_-$ , we get

$$t_{+}^{0} = \frac{v_{+} - v_{0}}{v_{+} - v_{-}}. (14)$$

The absence of  $z_j$  in eqn (14), in spite of their presence in the definition of  $t_+^0$  in eqn (13), is noteworthy. In other words, the expression for  $t_+^0$  for multivalent ions is identical to that for univalent ions (eqn (3)).

The fact that  $\rho_+$  reduces to  $t_+^0$  in the limit of infinite dilution for both univalent and multivalent ions was proved in ref. 22. This is the justification for eqn (1). Eqn (2) is obtained by replacing the Stefan–Maxwell diffusion coefficients in eqn (13) by self-diffusion coefficients. Thus, we have justified all of the equations presented in the introduction.

In concentrated solution theory, conductivity,  $\kappa$ , is given by (eqn (12.23) in ref. 12):

$$\frac{1}{\kappa} = -\frac{RT}{c_{\rm T}z_{+}z_{-}F^{2}} \left( \frac{1}{\mathcal{D}_{+-}} + \frac{c_{0}t_{-}^{0}}{c_{+}\mathcal{D}_{0-}} \right) \tag{15}$$

Substituting eqn (6) and (9) into eqn (15) gives (after some algebra)

$$\kappa = \frac{cz_{+}\nu_{+}(\nu_{-} - \nu_{+})}{\nabla \phi} = \frac{c_{+}z_{+}(\nu_{-} - \nu_{+})}{\nabla \phi}.$$
 (16)

Note that in Fig. 3, we assume that  $\nabla \phi$  is negative. While we conduct eNMR experiments at different values of  $\nabla \phi$ , all of the reported species velocities are scaled to  $\nabla \phi = -1 \text{ V mm}^{-1}$ . In this case we expect  $\nu_+$  to be positive and  $\nu_-$  to be negative if the salt dissociates into free anions and cations. The two velocities thus make additive contributions to  $\kappa$  which is always positive.

Eqn (14) and (16) are the main results of our analysis. We will use these equations along with eqn (1) and (2) to analyze data from our POSS-PSLiTFSI/EC/DMC electrolyte. While velocities depend on the reference frame used to measure them, they appear in eqn (14) and (16) in combinations that are independent of the reference frames. Our treatment assumes that the solutions contain 3 species: cations, anions and solvents. We ignore the polydispersity of the anion. We also ignore the complications arising from the presence of a mixture of solvents.

## Results and discussion

Fig. 4 shows the concentration dependence of the PFG-NMRbased self-diffusion coefficients of the four species of interest, the  $Li^{+}$  cation, the POSS-PSTFSI<sup>20-</sup>, EC, and DMC ( $D_{+}$ ,  $D_{-}$ ,  $D_{0,EC}$  and  $D_{0,\text{DMC}}$ ). We have chosen  $c_+$ , the molar concentration of Li<sup>+</sup> ions per unit volume of solution, as a measure of salt concentration. Note that  $c_+$  appears naturally in the expression for conductivity (see eqn (16)). The overall trends seen in Fig. 4 are not surprising. The solvent diffusion coefficients are largest, followed by  $D_+$  which is significantly higher than  $D_{-}$  at all salt concentrations. Some of the differences in ion self-diffusion coefficients can be explained by the difference in molar masses of Li<sup>+</sup> (7 g mol<sup>-1</sup>) and POSS-PSTFSI<sup>20-</sup> (10 648 g mol<sup>-1</sup>). Note however that in the dilute limit,  $D_{+}$  is only a factor of 2 larger than  $D_{-}$ . One might expect a larger factor based on the ratio of molar masses (1500). The PFG-NMR data suggest the presence of complex interactions between ions. The diffusion of Li<sup>+</sup> is slower than that of the solvents in spite of the fact that the solvent molecules have larger molar masses. This effect, which arises due to coordination between Li<sup>+</sup> and solvent molecules, is consistent with all previous PFG-NMR studies of

electrolytes. 18,20 The diffusion coefficients of all the species decrease with the increasing salt concentration due to an increase in frictional interactions.  $^{20,50}$  While  $D_{+}$  decreases more-or-less linearly by a factor of 5,  $D_{-}$  decreases more sharply when  $c_{+}$ exceeds 0.40 mol  $L^{-1}$ . The overall decrease in  $D_{-}$  over our concentration window is a factor of 20. One might expect the dependence of  $D_{-}$  on the concentration in the dilute limit, wherein the anions are widely spaced, to be different from that in the semi-dilute regime, wherein the anions overlap with each other. If we assume that the crossover from dilute to semi-dilute occurs at  $c_{+}^{*} = 0.40 \,\text{mol}\,L^{-1}$  (i.e.,  $c_{-}^{*} = 0.40/20 = 0.02 \,\text{mol}\,L^{-1}$ ), the size (length R) of the anion is estimated to be 4.4 nm,  $R = (N_{AV}c_{-}^{*})^{-1/3}$ , where  $N_{AV}$  is Avogadro's number. This is commensurate with the chemical structure shown in Fig. 1, suggesting that the star-shaped anions are "entangled" with each other in the  $c_+ > 0.40$  mol L<sup>-1</sup> concentration range. We will use the data in Fig. 4 in conjunction with eqn (2) to obtain the concentration dependence of  $t_{+,PFG}$ .

Fig. 5 shows the concentration dependence of the eNMRbased electric-field induced species velocities at -1 V mm<sup>-1</sup> of the four species of interest: the Li<sup>+</sup> cation, the POSS-PSTFSI<sup>20-</sup>, EC, and DMC  $(\nu_+, \nu_-, \nu_{0,EC})$  and  $\nu_{0,DMC}$ . Both the cation  $(\nu_+)$ and polyanion  $(\nu_{-})$  velocities are negative at all electrolyte concentrations: the cations migrate towards the positive electrode under the applied electric field. The magnitudes of these velocities decrease with the increasing concentration, consistent with the increase in frictional interactions. While the solvent velocities ( $\nu_{0,EC}$  and  $\nu_{0,DMC}$ ) are close to zero at all concentrations, the magnitudes of  $v_+$  and  $v_-$  decrease with salt concentration up to  $c_+ = 0.40 \text{ mol L}^{-1}$ . At  $c_+ = 0.40 \text{ mol L}^{-1}$ ,  $\nu_{+}$  approaches zero and is comparable to the solvent velocity.

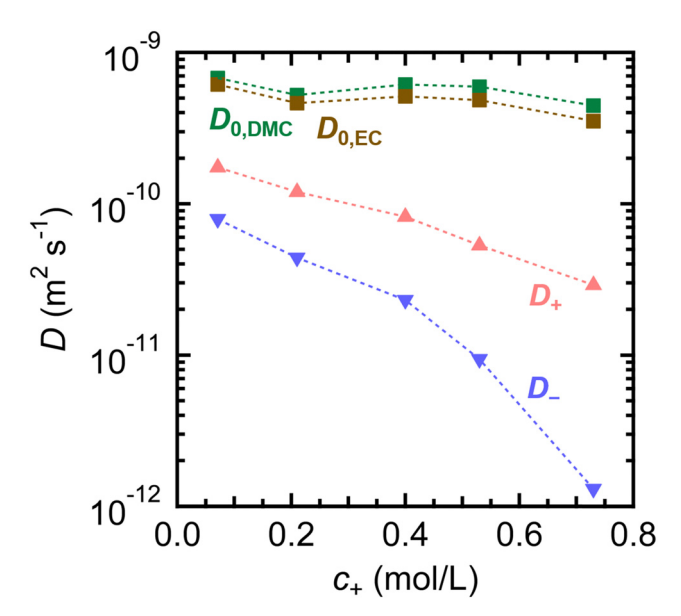


Fig. 4 Self-diffusion coefficients of cations (up triangle, pink), polyanions (down triangle, blue) and solvents (square, green for DMC and square, brown for EC) measured by PFG-NMR as a function of the salt concentration at 30 °C.

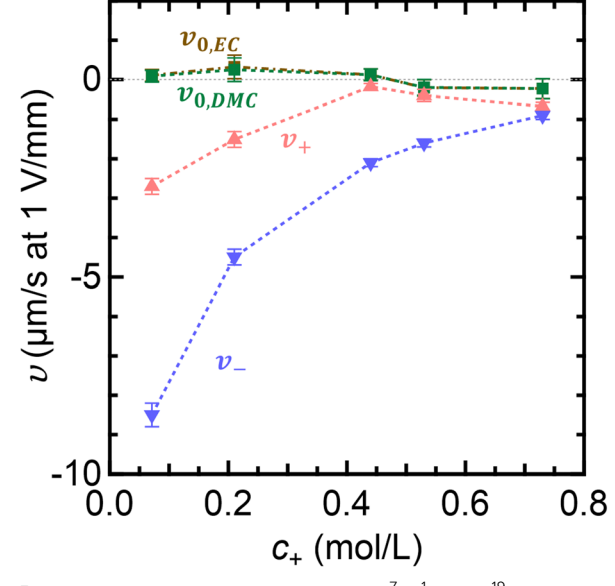


Fig. 5 Average species velocities measured by <sup>7</sup>Li, <sup>1</sup>H, and <sup>19</sup>F electrophoretic NMR (eNMR) at 30 °C as a function of the salt concentration, cation velocity (up triangle, red), polyanion velocity (down triangle, blue) and solvent velocities (square, green for DMC and square, brown for EC) at an applied field of  $\nabla \phi = -1 \, \text{V mm}^{-1}$ 

Increasing  $c_+$  further to 0.53 mol L<sup>-1</sup> results in a slight increase in the magnitude of  $\nu_+$ . In contrast, the magnitude of  $\nu_$ decreases monotonically throughout our concentration window. At the highest salt concentration,  $c_{+} = 0.73 \text{ mol L}^{-1}$ , we arrive at the interesting situation where  $\nu_+ \approx \nu_-$ ; both the magnitudes and the signs of the ion velocities are identical (or nearly so).

In Fig. 6, we plot the ac-impedance-based conductivity,  $\kappa$ , as a function of the salt concentration. The increase in  $\kappa$  with increasing  $c_+$  at low concentrations ( $c_+$  < 0.40 mol L<sup>-1</sup>) is due to an increase in the charge carrier concentration. However, frictional interactions also increase with increasing  $c_+$ . Above  $c_{+} = 0.40 \text{ mol L}^{-1}$ , the increase in frictional interactions dominates and  $\kappa$  decreases with the increasing concentration. These data are consistent with the extensive literature of monovalent salts dissolved in solvents. 20,51,52 We can also calculate  $\kappa$  using the eNMR data in Fig. 5 and eqn (16). These values are also shown in Fig. 6. The agreement is reasonable at all concentrations. Our theoretical framework, which is based on concentrated solution theory of binary electrolytes, does not account for the polydispersity of the salt. For example, eqn (16), used to calculate  $\kappa$  from the eNMR data, is an approximation for a polydisperse system. Eqn (16) is derived from eqn (15) assuming a fixed value of  $z_{-}$ , whereas polydispersity will lead to a range of values. We posit that the deviations between the two sets of data in Fig. 6 are due to this.

Fig. 7 compares cation transference numbers using the three independent methods. The current fraction value  $(\rho_+)$ , measured electrochemically, is found to be constant around 0.55 for all salt concentrations except at the highest salt concentration, where the value decreases slightly to 0.51. This suggests that lithium transference decreases only slightly as  $c_{+}$  increases from 0.53 to 0.73 mol L<sup>-1</sup>. The fact that

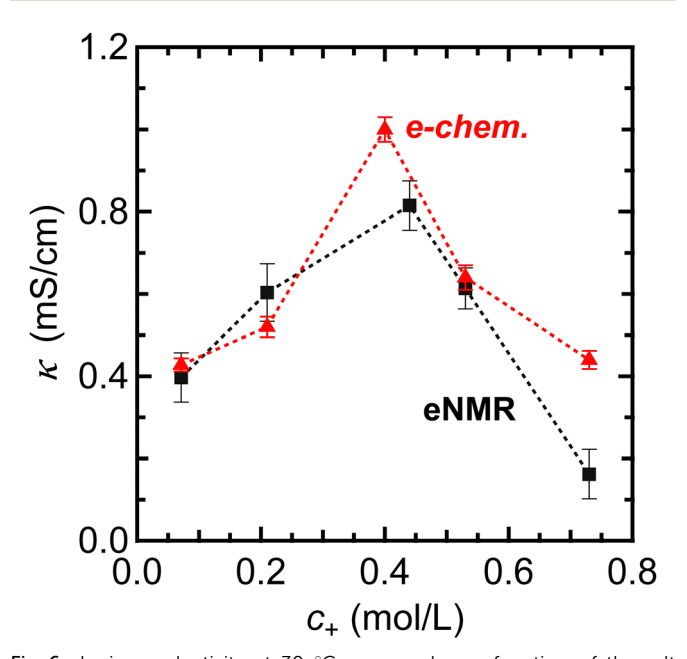


Fig. 6 Ionic conductivity at 30 °C measured as a function of the salt concentration using two independent methods: an electrochemical method (up triangle, red) and an eNMR method (square, black).

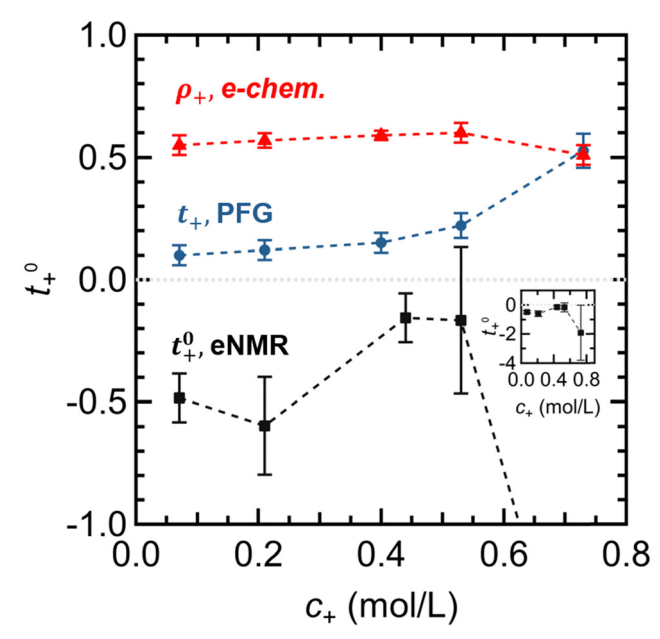


Fig. 7 Comparison of the transference number measured as a function of the salt concentration at 30 °C using three independent methods. The current fraction  $(\rho_+)$  measured electrochemically (up triangle, red), the transference number measured using the PFG-NMR method ( $t_{+,PFG}$ ) (circle, blue) and the transference number measured using the eNMR technique ( $t_{+}^{0}$ ) (square, black). The inset represents  $t_{+}^{0}$  at the highest salt concentration

this value is significantly higher than values obtained with univalent lithium salts, which range between 0.3 and 0.4, 8,29,51,53,54 suggests that lithium transference has generally improved due to the presence of the bulky POSS-PSTFSI<sup>20-</sup>. The transference number measured using the PFG-NMR  $(t_{+,PFG})$ method is 0.15 in the  $c_{+} \leq 0.40 \text{ mol L}^{-1}$  regime and increases sharply to overlap with  $\rho_+$  at  $c_+$  = 0.73 mol L<sup>-1</sup>. This observation by itself suggests that lithium transference increases sharply when  $c_{+}$  increases from 0.53 to 0.73 mol L<sup>-1</sup>, a conclusion which is at odds with that based on  $\rho_+$ . At most concentrations, the current supported by our electrolyte is significantly higher than that expected from  $t_{+,PFG}$ . It is obvious that the motion of ions under an applied potential is very different from the selfdiffusion of ions in the absence of an applied potential.

The last measure of cation transference that we wish to discuss is  $t_{+}^{0}$ . We calculate this quantity using eqn (14), assuming that  $v_0$  is the average velocity of the two solvents. The surprising result is that  $t_{+}^{0}$  is negative at all salt concentrations, a result that cannot be anticipated from either steady-state current measurements or PFG-NMR. This finding is consistent with negative transference numbers observed by eNMR in analogous liquid electrolytes.<sup>23</sup> A quantitative molecular level understanding of the differences between  $t_+^0$ ,  $\rho_+$  and  $t_{+,PFG}$  is outside the scope of this paper. The fact that they differ substantially from each other across the concentration range studied indicates that our data are well-removed from the infinite dilution limit where agreement between the 3 parameters is expected.21 In an attempt to provide a qualitative explanation for negative  $t_{+}^{0}$  values, we posit that the Li<sup>+</sup> counterions are in two states: a fraction of the ions f are fully dissociated and migrate freely under the electric field in

the +x direction, while the remainder are tightly coordinated with the anions in accordance with the principle of Manning condensation,  $^{55-59}$  and migrate with anions in the -x direction (Fig. 3). Let us call the migration velocity of the free cations  $v_{f+}$ . The measured value of  $v_+$  reflects a weighted average of these two populations:

$$v_{+} = f v_{f^{+}} + (1 - f) v_{-} \tag{17}$$

The negative value of  $t_{+}^{0}$  indicates that the overall mobility of the cations is dominated by the condensed counterions, implying that the second term on the right side of eqn (17), which we expect to be negative, is larger in magnitude than the first term. Assuming  $v_0 \approx 0$  (Fig. 5) for simplicity,  $t_+^0$  defined by eqn (14) is given by

$$t_{+}^{0} = \frac{f v_{f+} + (1 - f) v_{-}}{f v_{f+} + (1 - f) v_{-} - v_{-}}$$
(18)

Eqn (18) contains two unknown parameters, f and  $v_{f+}$ , and we expect both parameters to be functions of  $c_+$ . The measurement of cation transference alone does not permit determining both these parameters. Detailed computer simulations and additional experiments are necessary to test the validity of our hypothesis and provide a consistent explanation for the observed relationships between  $\rho_+$ ,  $t_{+,PFG}$  and  $t_+^0$ . In this preliminary analysis, we mainly want to show that this framework provides a reasonable explanation for our observations of negative  $t_{+}^{0}$ . For example, at  $c_{+} = 0.071$  mol L<sup>-1</sup>, if we assume f = 0.5 then the measured values of  $t_{+}^{0}$  and  $v_{-}$  give  $v_{f+} = 3 \mu \text{m s}^{-1}$ based on eqn (18). This value of  $v_{f+}$  is positive, and several times smaller in magnitude than the anion velocity, which is consistent with eNMR measurements of fully dissociated electrolytes. 25 In Fig. S1 in the ESI,† we provide values for  $v_{f+}$ for other possible values of f.

Conductivity is proportional to the difference between the cation and anion velocities (eqn (16)). In most electrolytes, these velocities are in the opposite directions, resulting in additive contributions to the conductivity. We have shown that this is not the case for POSS-PSTFSI<sup>20-</sup>-based electrolytes. Here,  $\nu_+$  and  $\nu_-$  are both negative at all values of  $c_+$  and thus the ion velocities do not contribute additively to conductivity. At  $c_{+}$  = 0.73 mol L<sup>-1</sup>, we find that  $\nu_+ \approx \nu_-$ , and our analysis gives a value of -2 for  $t_{+}^{0}$ . There is, however, significant uncertainty due to the fact that the denominator of eqn (14) approaches zero. Using standard error propagation, we obtain  $t_{+}^{0} = -2 \pm 2$  at  $c_{+} =$ 0.73 mol L<sup>-1</sup>. Molecular dynamics simulations may provide some insight into this unusual case.

#### Conclusions

We studied lithium transference in a multivalent electrolyte containing a bulky star-shaped anion with  $z_{-} = -20$  using three experimental techniques: electrochemical polarization  $(\rho_+)$ , PFG-NMR  $(t_{+,PFG})$  and electrophoretic NMR  $(t_{+}^{0})$ . Interest in such electrolytes arises due to the possibility of improving lithium transference by slowing down the mobility of the anion. In univalent electrolytes, the self-diffusion coefficient of lithium

ions is much smaller than that of the anions. In our multivalent electrolyte, PFG-NMR shows that the reverse is true - the selfdiffusion coefficient of the cation is higher than that of the anions at all salt concentrations. Electrochemical polarization experiments show that the multivalent electrolytes are able to sustain a higher current than that expected from PFG-NMR. The cation transference number with respect to the solvent velocity,  $t_{+}^{0}$ , is negative at all salt concentrations indicating that cation transference does not necessarily reflect the slowing down of the self-diffusion coefficient of the anion. Similar effects were reported by Fong et al. in solutions of linear multivalent anions with lithium counterions. 19,60 Recently, using eNMR, Bergstrom et al. showed that  $t_{+}^{0}$  was negative for these systems.<sup>23</sup> It is evident that ion transport in our multivalent electrolytes depends on additional parameters such as the activity of the multivalent salt, and the diffusion coefficient measured by approaches such as restricted diffusion. In addition, computer simulations that account for anion-solvent, cation-solvent and cation-anion correlations are necessary to understand the molecular underpinnings of ion transport in electrolytes with multivalent star-shaped ions.

### **Author contributions**

The manuscript was written through contributions of all authors. All the authors gave approval to the final version of the manuscript. S. C. and D. M. H. contributed equally.

### Conflicts of interest

There are no conflicts of interest to declare.

# Acknowledgements

This work was fully supported by the Joint Center for Energy Storage Research (JCESR), an Energy Innovation Hub funded by the U.S. Department of Energy, Office of Science, Basic Energy Sciences (Contract DE-AC02-06CH11357). We thank Dr Hasan Celik and UC Berkeley's NMR facility in the College of Chemistry (CoC-NMR) for spectroscopic assistance. The NMR instrument used in this work was supported by the National Science Foundation under grant no. 2018784. We thank Helen Bergstrom for helpful scientific input.

## References

- 1 T. K. L. Nguyen, T. N. T. Phan, F. Cousin, D. Devaux, S. Mehan, F. Ziarelli, S. Viel, D. Gigmes, P. Soudant and R. Bouchet, Polyhedral Oligomeric Silsesquioxane-Based Macroanions to Level Up the Li<sup>+</sup> Transport Number of Electrolytes for Lithium Batteries, Chem. Mater., 2022, 34, 6944-6957.
- 2 R. M. Darling, K. G. Gallagher, J. A. Kowalski, S. Ha and F. R. Brushett, Pathways to Low-Cost Electrochemical

- Energy Storage: A Comparison of Aqueous and Nonaqueous Flow Batteries, Energy Environ. Sci., 2014, 7, 3459-3477.
- 3 K. E. Rodby, T. J. Carney, Y. Ashraf Gandomi, J. L. Barton, R. M. Darling and F. R. Brushett, Assessing the Levelized Cost of Vanadium Redox Flow Batteries with Capacity Fade and Rebalancing, I. Power Sources, 2020, 460, 227958.
- 4 K.-C. Lau, T. J. Seguin, E. V. Carino, N. T. Hahn, J. G. Connell, B. J. Ingram, K. A. Persson, K. R. Zavadil and C. Liao, Widening Electrochemical Window of Mg Salt by Weakly Coordinating Perfluoroalkoxyaluminate Anion for Mg Battery Electrolyte, J. Electrochem. Soc., 2019, 166, A1510-A1519.
- 5 N. T. Hahn, S. A. McClary, A. T. Landers and K. R. Zavadil, Efficacy of Stabilizing Calcium Battery Electrolytes through Salt-Directed Coordination Change, J. Phys. Chem. C, 2022, **126**, 10335-10345.
- 6 J. Self, N. T. Hahn, K. D. Fong, S. A. McClary, K. R. Zavadil and K. A. Persson, Ion Pairing and Redissociaton in Low-Permittivity Electrolytes for Multivalent Battery Applications, J. Phys. Chem. Lett., 2020, 11, 2046-2052.
- 7 A. Nyman, M. Behm and G. Lindbergh, Electrochemical Characterisation and Modelling of the Mass Transport Phenomena in LiPF<sub>6</sub>-EC-EMC Electrolyte, *Electrochim. Acta*, 2008, 53, 6356-6365.
- 8 J. Landesfeind and H. A. Gasteiger, Temperature and Concentration Dependence of the Ionic Transport Properties of Lithium-Ion Battery Electrolytes, J. Electrochem. Soc., 2019, 166, A3079-A3097.
- 9 O. E. Geiculescu, R. Rajagopal, S. E. Creager, D. D. DesMarteau, X. Zhang and P. Fedkiw, Transport Properties of Solid Polymer Electrolytes Prepared from Oligomeric Fluorosulfonimide Lithium Salts Dissolved in High Molecular Weight Poly(Ethylene Oxide), J. Phys. Chem. B, 2006, 110, 23130-23135.
- 10 K. D. Kreuer, A. Wohlfarth, C. C. Araujo, A. Fuchs and J. Maier, Single Ion Li<sup>+</sup> Na<sup>+</sup> Conductors by Ion Exchange of Proton-Conducting Ionomers and Polyelectrolytes, Chem. Phys. Chem., 2011, 12, 2558.
- 11 B. Qiao, G. M. Leverick, W. Zhao, A. H. Flood, J. A. Johnson and Y. Shao-Horn, Supramolecular Regulation of Anions Enhances Conductivity and Transference Number of Lithium in Liquid Electrolytes, J. Am. Chem. Soc., 2018, 140, 10932-10936.
- 12 J. Newman and N. P. Balsara, Electrochemical Systems, Wiley, Hoboken, 4th edn, 2021.
- 13 L. Onsager, Reciprocal Relations in Irreversible Processes. I, Phys. Rev., 1931, 37, 405.
- 14 L. Onsager, Reciprocal Relations in Irreversible Processes. II, Phys. Rev., 1931, 38, 2265.
- 15 P. G. Bruce and C. A. Vincent, Steady State Current Flow in Solid Binary Electrolyte Cells, J. Electroanal. Chem., 1987, 225, 1-17.
- 16 J. Evans, C. A. Vincent and P. G. Bruce, Electrochemical Measurement of Transference Numbers in Polymer Electrolytes, Polymer, 1987, 28, 2324-2328.
- 17 M. Watanabe, S. Nagano, K. Sanui and N. Ogata, Estimation of Li<sup>+</sup> Transport Number in Polymer Electrolytes by the

- Combination of Complex Impedance and Potentiostatic Polarization Measurements, Solid State Ionics, 1988, 30, 911-917.
- 18 K. Hayamizu, E. Akiba, T. Bando and Y. Aihara, <sup>1</sup>H, <sup>7</sup>Li, and <sup>19</sup>F Nuclear Magnetic Resonance and Ionic Conductivity Studies for Liquid Electrolytes Composed of Glymes and Polyetheneglycol Dimethyl Ethers of CH<sub>3</sub>O(CH<sub>2</sub>CH<sub>2</sub>O)<sub>n</sub>CH<sub>3</sub> (n = 3 - 50) Doped with LiN(SO<sub>2</sub>CF<sub>3</sub>)<sub>2</sub>, *J. Chem. Phys.*, 2002, 117, 5929-5939.
- 19 K. D. Fong, J. Self, K. M. Diederichsen, B. M. Wood, B. D. McCloskey and K. A. Persson, Ion Transport and the True Transference Number in Nonaqueous Polyelectrolyte Solutions for Lithium Ion Batteries, ACS Cent. Sci., 2019, 5, 1250-1260.
- 20 L. S. Grundy, D. B. Shah, H. O. Nguyen, K. M. Diederichsen, H. Celik, J. M. DeSimone, B. D. McCloskey and N. P. Balsara, Impact of Frictional Interactions on Conductivity, Diffusion, and Transference Number in Ether- and Perfluoroether-Based Electrolytes, J. Electrochem. Soc., 2020, 167, 120540.
- 21 K. W. Gao, C. Fang, D. M. Halat, A. Mistry, J. Newman and N. P. Balsara, The Transference Number, Energy Environ. Mater., 2022, 5, 366-369.
- 22 N. P. Balsara and J. Newman, Divergence of Velocity Fields in Electrochemical Systems, J. Electrochem. Soc., 2022, **169**, 070535.
- 23 H. K. Bergstrom, K. D. Fong, D. M. Halat, C. A. Karouta, H. C. Celik, J. A. Reimer and B. D. McCloskey, Ion Correlation and Negative Lithium Transference in Polyelectrolyte Solutions, Chem. Sci., 2023, 14, 6546-6557.
- 24 K. Timachova, J. Newman and N. P. Balsara, Theoretical Interpretation of Ion Velocities in Concentrated Electrolytes Measured by Electrophoretic NMR, J. Electrochem. Soc., 2019, 166, A264-A267.
- 25 D. M. Halat, C. Fang, D. Hickson, A. Mistry, J. A. Reimer, N. P. Balsara and R. Wang, Electric-Field-Induced Spatially Dynamic Heterogeneity of Solvent Motion and Cation Transference in Electrolytes, Phys. Rev. Lett., 2022, 128, 198002.
- 26 M. Giesecke, G. Mériguet, F. Hallberg, Y. Fang, P. Stilbs and I. Furó, Ion Association in Aqueous and Non-Aqueous Solutions Probed by Diffusion and Electrophoretic NMR, Phys. Chem. Chem. Phys., 2015, 17, 3402-3408.
- 27 H. Dai and T. A. Zawodzinski, The Dependence of Lithium Transference Numbers on Temperature, Salt Concentration and Anion Type in Poly (Vinylidene Fluoride)-Hexafluoropropylene Copolymer-Based Gel Electrolytes, J. Electroanal. Chem., 1998, 459, 111-119.
- 28 H. J. Walls and T. A. Zawodzinski, Anion and Cation Transference Numbers Determined by Electrophoretic NMR of Polymer Electrolytes Sum to Unity, Electrochem. Solid-State Lett., 2000, 3, 321-324.
- 29 F. Schmidt and M. Schönhoff, Solvate Cation Migration and Ion Correlations in Solvate Ionic Liquids, J. Phys. Chem. B, 2020, 124, 1245-1252.
- 30 A. A. Wang, A. B. Gunnarsdóttir, J. Fawdon, M. Pasta, C. P. Grey and C. W. Monroe, Potentiometric MRI of a Superconcentrated Lithium Electrolyte: Testing the

- Irreversible Thermodynamics Approach, ACS Energy Lett., 2021, 6, 3086-3095.
- 31 M. Brinkkötter, G. A. Giffin, A. Moretti, S. Jeong, S. Passerini and M. Schönhoff, Relevance of Ion Clusters for Li Transport at Elevated Salt Concentrations in [Pyr<sub>12O1</sub>][FTFSI] Ionic Liquid-Based Electrolytes, Chem. Commun., 2018, 54, 4278-4281.
- 32 P. Nürnberg, J. Atik, O. Borodin, M. Winter, E. Paillard and M. Schönhoff, Superionicity in Ionic-Liquid-Based Electrolytes Induced by Positive Ion-Ion Correlations, J. Am. Chem. Soc., 2022, 144, 4657-4666.
- 33 Q. R. Huang, P. L. Dubin, C. N. Moorefield and G. R. Newkome, Counterion Binding on Charged Spheres: Effect of pH and Ionic Strength on the Mobility of Carboxyl-Terminated Dendrimers, J. Phys. Chem. B, 2000, 104, 898-904.
- 34 E. Sevrek, P. L. Dubin and G. R. Newkome, Effect of Electric Field on the Mobility of Carboxyl-Terminated Dendrimers, J. Phys. Chem. B, 2004, 108, 10168-10171.
- 35 J.-P. Hsu, C.-Y. Lin, L.-H. Yeh and S.-H. Lin, Influence of the Shape of a Polyelectrolyte on Its Electrophoretic Behavior, Soft Matter, 2012, 8, 9469-9479.
- 36 P. P. Gopmandal and S. Bhattacharyya, Nonlinear Effects on Electrokinetics of a Highly Charged Porous Sphere, Colloid Polym. Sci., 2014, 292, 905-914.
- 37 C. F. Welch and D. A. Hoagland, The Electrophoretic Mobility of PPI Dendrimers: Do Charged Dendrimers Behave as Linear Polyelectrolytes or Charged Spheres?, Langmuir, 2003, 19, 1082-1088.
- 38 M. Moussa, C. Caillet, R. M. Town and J. F. L. Duval, Remarkable Electrokinetic Features of Charge-Stratified Soft Nanoparticles: Mobility Reversal in Monovalent Aqueous Electrolyte, Langmuir, 2015, 31, 5656-5666.
- 39 I. Villaluenga, X. C. Chen, D. Devaux, D. T. Hallinan and N. P. Balsara, Nanoparticle-Driven Assembly of Highly Conducting Hybrid Block Copolymer Electrolytes, Macromolecules, 2015, 48, 358-364.
- 40 W. M. Spees, S.-K. Song, J. R. Garbow, J. J. Neil and J. J. H. Ackerman, Use of Ethylene Glycol to Evaluate Gradient Performance in Gradient-Intensive Diffusion MR Sequences, Magn. Reson. Med., 2012, 68, 319-324.
- 41 Y. Fang, P. V. Yushmanov and I. Furó, Improved Accuracy and Precision in Electrophoretic NMR Experiments. Current Control and Sample Cell Design, J. Magn. Reson., 2020, 318, 106796.
- 42 A. Jerschow and N. Müller, Convection Compensation in Gradient Enhanced Nuclear Magnetic Resonance Spectroscopy, J. Magn. Reson., 1998, 132, 13-18.
- 43 Q. He and Z. Wei, Convection Compensated Electrophoretic NMR, J. Magn. Reson., 2001, 150, 126-131.
- 44 E. Pettersson, I. Furó and P. Stilbs, On Experimental Aspects of Electrophoretic NMR, Concepts Magn. Reson., Part A: Bridging Educ. Res., 2004, 22, 61-68.
- 45 Z. Zhang and L. A. Madsen, Observation of Separate Cation and Anion Electrophoretic Mobilities in Pure Ionic Liquids, J. Chem. Phys., 2014, 140, 084204.

- 46 D. R. Wheeler and J. Newman, Molecular Dynamics Simulations of Multicomponent Diffusion. 1. Equilibrium Method, J. Phys. Chem. B, 2004, 108, 18353-18361.
- 47 A. France-Lanord and J. C. Grossman, Correlations from Ion Pairing and the Nernst-Einstein Equation, Phys. Rev. Lett., 2019, 122, 136001.
- 48 K. D. Fong, H. K. Bergstrom, B. D. McCloskey and K. K. Mandadapu, Transport Phenomena in Electrolyte Solutions: Nonequilibrium Thermodynamics and Statistical Mechanics, AIChE J., 2020, 66, e17091.
- 49 C. Fang, A. Mistry, V. Srinivasan, N. P. Balsara and R. Wang, Elucidating the Molecular Origins of the Transference Number in Battery Electrolytes Using Computer Simulations, JACS Au, 2023, 3, 306-315.
- 50 K. I. S. Mongcopa, D. A. Gribble, W. S. Loo, M. Tvagi, S. A. Mullin and N. P. Balsara, Segmental Dynamics Measured by Quasi-Elastic Neutron Scattering and Ion Transin Chemically Distinct Polymer Electrolytes, Macromolecules, 2020, 53, 2406-2411.
- 51 D. T. Hickson, D. M. Halat, A. S. Ho, J. A. Reimer and N. P. Balsara, Complete Characterization of a Lithium Battery Electrolyte Using a Combination of Electrophoretic NMR and Electrochemical Methods, Phys. Chem. Chem. Phys., 2022, 24, 26591-26599.
- 52 K. Yoshida, M. Tsuchiya, N. Tachikawa, K. Dokko and M. Watanabe, Change from Glyme Solutions to Quasi-Ionic Liquids for Binary Mixtures Consisting of Lithium Bis(Trifluoromethanesulfonyl)Amide and Glymes, J. Phys. Chem. C, 2011, 115, 18384-18394.
- 53 T. Hou and C. W. Monroe, Composition-Dependent Thermodynamic and Mass-Transport Characterization of Lithium Hexafluorophosphate in Propylene Carbonate, Electrochim. Acta, 2020, 332, 135085.
- 54 N. Craig, S. A. Mullin, R. Pratt and G. B. Crane, Determination of Transference Number and Thermodynamic Factor by Use of Anion-Exchange Concentration Cells and Concentration Cells, J. Electrochem. Soc., 2019, 166, A2769-A2775.
- 55 G. S. Manning, Nonconvective Ionic Flow in Fixed-Charge Systems, J. Chem. Phys., 1967, 46, 2324-2333.
- 56 G. S. Manning, Limiting Laws and Counterion Condensation in Polyelectrolyte Solutions II. Self-Diffusion of the Small Ions, J. Chem. Phys., 1969, 51, 934-938.
- 57 G. S. Manning, Molecular Theory of Counterion Conductivity and Self-Diffusion in Polyelectrolyte Solutions, J. Chem. Phys., 1967, 47, 2010-2013.
- 58 U. Böhme and U. Scheler, Effective Charge of Poly(Styrenesulfonate) and Ionic Strength - An Electrophoresis NMR Investigation, Colloids Surf., A, 2003, 222, 35-40.
- 59 U. Böhme, A. Klenge, B. Hänel and U. Scheler, Counterion Condensation and Effective Charge of PAMAM Dendrimers, Polymers, 2011, 3, 812-819.
- 60 K. D. Fong, J. Self, B. D. McCloskey and K. A. Persson, Ion Correlations and Their Impact on Transport in Polymer-Based Electrolytes, Macromolecules, 2021, 54, 2575-2591.